Title

Age-related neurochemical changes in the rhesus macaque superior olivary complex

Journal

The Journal of Comparative Neurology, 522(3)

ISSN

1550-7149

Authors

Gray, Daniel T
Engle, James R
Recanzone, Gregg H

Publication Date

2014-02-15

DOI

10.1002/cne.23427

Peer reviewed

Published in final edited form as:
J Comp Neurol. ; 522(3): 573–591.

Age-Related Neurochemical Changes in the Rhesus Macaque Superior Olivary Complex

Daniel T. Gray[1], **James R. Engle**[2], and **Gregg H. Recanzone**[1,3,*]

[1]Center for Neuroscience, University of California at Davis, Davis, California 95616

[2]Evelyn F. McKnight Brain Institute, University of Arizona, Tucson, Arizona 85721

[3]Department of Neurobiology, Physiology and Behavior, University of California at Davis, Davis, California 95616

Abstract

Positive immunoreactivity to the calcium-binding protein parvalbumin (PV) and nitric oxide synthase NADPH-diaphorase (NADPHd) is well documented within neurons of the central auditory system of both rodents and primates. These proteins are thought to play roles in the regulation of auditory processing. Studies examining the age-related changes in expression of these proteins have been conducted primarily in rodents but are sparse in primate models. In the brainstem, the superior olivary complex (SOC) is crucial for the computation of sound source localization in azimuth, and one hallmark of age-related hearing deficits is a reduced ability to localize sounds. To investigate how these histochemical markers change as a function of age and hearing loss, we studied eight rhesus macaques ranging in age from 12 to 35 years. Auditory brainstem responses (ABRs) were obtained in anesthetized animals for click and tone stimuli. The brainstems of these same animals were then stained for PV and NADPHd reactivity. Reactive neurons in the three nuclei of the SOC were counted, and the densities of each cell type were calculated. We found that PV and NADPHd expression increased with both age and ABR thresholds in the medial superior olive but not in either the medial nucleus of the trapezoid body or the lateral superior olive. Together these results suggest that the changes in protein expression employed by the SOC may compensate for the loss of efficacy of auditory sensitivity in the aged primate.

Indexing Terms

NADPH-diaphorase; parvalbumin; brainstem; ABR; monkey; geriatric; aging

*CORRESPONDENCE TO: Gregg H. Recanzone, Center for Neuroscience, 1544 Newton Ct., Davis, CA 95618. ghrecanzone@ucdavis.edu.

Conflicts Of Interest Statement: The authors declare no conflicts of interest.

Role of Authors: All authors had full access to all the data in the study and take responsibility for the integrity of the data and the accuracy of the data analysis. Study concept and design: DTG, JRE, GHR. Acquisition of data: DTG, JRE. Analysis and interpretation of data: DTG, GHR. Drafting of the manuscript: DTG, GHR. Critical revision of the manuscript for important intellectual content: DTG, GHR. Statistical analysis: DTG. Obtained funding: JRE, GHR. Administrative, technical, and material support: DTG, JRE. Study supervision: GHR.

Age-related hearing loss is characterized by peripheral changes in the cochlea, and/or changes in central auditory processing (Schulte and Schmiedt, 1992; Spicer and Schulte, 2002; Engle et al., 2012). For example, the efficacy of GABAergic and glycinergic inhibitory mechanisms declines with age throughout the central auditory system (Caspary et al., 1995, 1999, 2005, 2006, 2008), and physiological studies in aged animals reveal varying degrees of degradation in the sound-processing abilities of aged neurons (Mendelson and Rickets, 2001; Palombi et al., 2001; Lee et al., 2002). Interestingly, the expression of calcium-binding proteins and nitric oxide synthases has also repeatedly been shown to change within the aging auditory system (O'Neill et al., 1997; Zettel et al., 1997; Ouda et al., 2003, 2008; Sanchez-Zuriaga et al., 2007; Huh et al., 2008). The vast majority of this work has been done in nonprimate models; however, physiological studies in primate auditory cortex suggest an analogous age-related release from inhibition and a broadening in the spatial tuning of neurons (Juarez-Salinas et al., 2010; Engle and Recanzone, 2012). Whether the underlying age-related chemical changes seen in the auditory system of rodents also exist in the macaque is unknown.

Parvalbumin (PV), like other calcium-binding proteins, serves primarily as a calcium buffer, regulating the levels of intracellular calcium. As with most neurotransmitters, γ-aminobutyric acid (GABA) release is calcium dependent (Tang et al., 2011), and distinct classes of interneurons in the cerebral cortex are described by their neurochemical signatures to calcium-binding proteins such as PV and calbindin, among others (Carder et al., 1996). Moreover, rodent cortical and hippocampal PV-expressing cells release GABA (Klausberger and Somogyi, 2008; Rudy et al., 2011; Bartos and Elgueta, 2012), so these cells are considered a major inhibitory interneuron class in these brain regions. The physiological activity and neurotransmission of subcortical PV-expressing neurons is less well understood, although PV is consistently found in the brainstem and midbrain. Along with neurotransmitter release, free calcium regulates numerous cellular processes, many of which are affected by aging. Examples of such processes include gene transcription, maintenance of cytoarchitecture, activation/deactivation of enzymatic activity, and various plastic changes associated with learning and memory (Disterhoft et al., 1995; Toescu and Vreugdenhil, 2010). Labeling of calcium buffers such as PV is therefore used to detect potential changes in calcium-dependent activity related to the aging processes.

NADPH-diaphorase (NADPHd) is a nitric oxide (NO) synthase (Bredt et al., 1991; Dawson et al., 1991a), and produces NO by deaminating the amino acid arginine. NO is found throughout the central nervous system as a signaling molecule and neuromodulator (for review see Esplugues, 2002). Along with these primary roles NO has been shown to help induce long-term depression in the cerebellum (Shibuki and Okada, 1991) and long-term potentiation in the hippocampus (Bon and Garthwaite, 2001, 2003). $NADPHd^+$ cells are consistently found throughout the auditory system; however, NO's role in audition beyond signaling and modulation remains unclear. $NADPHd^+$ cells potentially regulate and resist glutamate excitotoxicity (Dawson et al., 1991b). This resistance helps maintain a healthy intracellular environment and may prevent oversaturation of neural responses. Furthermore, the action of NADPHd is calcium dependent. These NADPHd proteins colocalize in cells with calcium-binding proteins and are physically coupled to N-methly-D-Aspartate (NMDA) receptors via the linker protein PSD-95, where NADPHd utilizes the high-calcium

environment surrounding these channels to produce NO (Bredt and Snyder 1990; Brenman et al., 1996; Fessenden and Schacht, 1998). NO also provides regulatory feedback to the NMDA receptor, along with its numerous signaling and modulatory actions (Hopper et al., 2004). Regardless of the exact purpose of NO in the auditory system, its relative expression consistently changes with age in rodents (Reuss et al., 2000; Ouda et al., 2003; Sanchez-Zuriaga et al., 2007; Huh et al., 2008), and, as with PV, primate studies exploring these changes are sparse (Udell et al., 2008).

We have recently begun investigating changes in primate NADPHd and PV expression of young and aged macaque monkeys. We have evidence of increases in PV^+ cell density in the central nucleus peripheral cortex of the inferior colliculus (IC) of aged monkeys compared with younger ones (unpublished observations). Interestingly, unlike the case in the rodent IC, NADPHd expression remained constant. These differences in age-related changes of NADPHd and PV expression within the IC raise the question of where along the ascending auditory pathway these changes originate or whether there is a simultaneous change in histochemistry across all ascending auditory nuclei.

The superior olivary complex (SOC) is a major input to the IC and is the first region to integrate information from each of the two cochlear nuclei (Webster, 1995; Oliver, 2000; Reuss, 2000; Tollin, 2003). The SOC processes binaural input critical for localization of sounds in azimuth. The medial superior olive (MSO) computes interaural time and phase differences (ITD and IPD, respectively), whereas the lateral superior olive (LSO) computes interaural level differences (ILD; Jeffress, 1948; Galambos et al., 1959; Boudreau and Tsuchitani, 1968; Guinan et al., 1972). The medial nucleus of the trapezoid body (MNTB) participates in sound localization processing by converting excitatory input from the contralateral CN into inhibitory glycernigic signals, then relaying them to the MSO and LSO (Yin and Chan, 1990; Brand et al., 2002; Tollin, 2003; Kulesza et al., 2007).

Several studies using auditory brainstem responses (ABR) note age-related hearing loss in the macaque (Torre and Fowler, 2000; Torre et al., 2004; Navarro et al., 2008; Fowler et al., 2010). The ABR is a useful diagnostic tool for peripheral hearing ability, because it is an estimation of auditory detection ability. However, it takes far fewer action potentials to detect a sound than it does to produce an ABR waveform. Evidence for this discrepancy lays in the observation that ABR thresholds are consistently 10–15 dB SPL higher than psychophysical hearing thresholds (for review see Stapells, 2000; Navarro et al., 2008), although audiograms generated by both methods retain the same overall shape. Interestingly, morphological features in the cochlea and IC correlate with changes in ABR thresholds of the macaque (Engle et al., 2013; unpublished observations).

Given the importance of calcium in the aging process and the repeated observation of age-related changes in PV and NADPHd in rodents, we investigated the age-related changes in the expression of these proteins in the SOC and their relationship to changes in the ABR of nonhuman primates. We obtained click and low-, middle-, and high-frequency ABRs and characterized the SOC for PV immunoreactivity and NADPHd histochemical reactions in monkeys varying in age between 12 years and 35 years. The MNTB, MSO, and LSO were examined separately to parse out changes in specific localization processes of the SOC and

were also combined to determine whether the changes of the nucleus as a whole are correlated with age and with ABR thresholds.

Materials and Methods

Stereological techniques were used to quantify the density of NADPHd-positive ($NADPHd^+$) and PV^+ cells in the SOC of young and aged rhesus macaques.

Animals

Table 1 gives the demographic information on the eight monkeys used in the study. The animals were included based on the following criteria: 1) no history of receiving ototoxic drugs; 2) no history of loud noise exposure or trauma to the ear; and 3) no outer ear occlusions or otitis media detected via otoscopic examination. Animals ranged in age from 12 to 35 years, which roughly corresponds in age to 37 to 107 human years (Davis and Leathers, 1985). The animals were maintained on ad libitum food and had free access to water. All procedures conformed to the National Institutes of Health guidelines for animal use and were approved by the UC Davis Institutional Animal Care and Use Committee.

ABR recording

ABRs were collected from all animals except for the 12 year old. To maintain chemical restraint during these non-noxious procedures, animals were given an initial dose of ketamine (10 mg/kg, i.m.) and medatomidine (0.3 ml/10 kg, i.m.) with supplemental doses of ketamine administered as needed throughout the procedure to maintain the appropriate level of chemical restraint. The animals were placed in the prone position with their heads slightly elevated inside either a double-walled acoustic chamber or in an electrically and acoustically quiet room. Two separate locations were used for the collection of ABRs because the animals were housed in different locations on the UC Davis campus. No differences were noted in recording quality between conditions. The ear canals were inspected, followed by an assessment of the state of the tympanic membrane. Otitis media was absent in all animals. The skin was cleaned with alcohol, and sterile stainless-steel wires (22 gauge) were placed subcutaneously behind both ears, on the forehead, and on the back of the neck (Allen and Starr, 1978; Torre and Fowler, 2000; Torre et al., 2004; Fowler et al., 2010). ABR waveforms were collected using an Intelligent Hearing System (Smart EP Win USB, version 3.97) controlled by a portable computer. The stimuli consisted of clicks and 10-msec (2-msec trapezoidal rise/fall) tone bursts (0.5, 1, 2, 4, 8, 12, 16 kHz) presented at a rate of 10 stimuli/second. Each stimulus was repeated a minimum of 1,000 times to obtain a reliable average ABR recording. All stimuli were first presented at 80 dB SPL and decreased by 10 dB increments until a clearly responsive ABR peak II and IV was no longer apparent. The intensity was then raised by 5 dB. The ABR threshold for a stimulus was interpolated between the two values that did and did not evoke a clear response at the given peak, i.e., within approximately 2.5 dB.

In accordance with previous studies, two independent observers, blind to the identity of the animals, analyzed and scored the amplitudes and latencies of the ABR peak waveforms (Laughlin et al., 1999). Amplitude was defined as the measure of the evoked potential from

the summit of the peak to the lowest point of the ensuing trough (Navarro et al., 2008). Latency was defined as the time from stimulus presentation to the summit of the peak. Observers scored peak II and IV latencies with an interobserver agreement greater than 95%.

Histological processing and antibody characterization

Animals were killed with a lethal dose of sodium pentobarbital (60 mg/kg, i.v.) and transcardially perfused with saline, a mixture of 4% paraformaldehyde and 0.1% glutaraldahyde in 0.1% phosphate buffer, and a mixture of 4% paraformaldehyde and 10% sucrose. The brains were extracted and cryoprotected in a mixture of 4% paraformaldehyde and 30% sucrose. Seven of the eight brains were cut perpendicular to the lateral sulcus at thicknesses ranging from 25 to 50 μm. In the final case, the thalamus, midbrain, and brainstem were separated from the neocortex and sliced in a rostral to caudal orientation at 50 μm. The tissue was washed and stored in 0.1% phosphate buffer (pH 7.4) prior to tissue processing (Hackett et al., 2001; de la Mothe et al., 2006a,b; Padberg et al., 2009). Alternate sections were stained for Nissl, PV immunohistochemistry, and NADPHd histochemistry (Scherer-Singler et al., 1983).

Immunohistochemical reactions followed a modified protocol of the ABC method (ABC kit; Vector, Burlingame, CA) and visualized with diaminobenzidine (DAB) or the Vector SG kit. Sections were blocked overnight in 3% normal horse serum (12 hours), then incubated in primary antibody (anti-PV in mouse, 1:4,000; Sigma-Aldrich, St. Louis, MO) for 4 hours, followed by a 1-hour incubation in the secondary antibody (biotinylated anti-mouse IgG, 1:250; Vector). Following several 5-minute rinses in 0.1 M PB, sections were incubated in a peroxidase substrate solution for visualization. NADPHd histochemistry utilizes the ability of this protein to reduce the dye nitroblue tetrazoluim into an insoluble formazan, visible via microscopy (Fessenden and Schacht, 1998). Sections were incubated for 1 hour in a solution of 1 mg/ml nitroblue tetrazoluim (Sigma Aldrich; N-6876), 0.5 mg/ml β-nicotinamide adenine dinucleotide phosphate (NADPH; Sigma-Aldrich; N-1630), and 0.1% Triton X-100 dissolved in 0.1 M phosphate buffer.

The isotype specificity of the anti-PV antibody was determined using the Sigma ImmunoType Kit (product code ISO-1), and by a double-diffusion immunoassay using mouse monoclonal antibody isotyping reagents (product code ISO-2). Negative controls in which either the primary antibody (PV immunohistochemistry) or the nitroblue tetrazolium (NADPHd histochemistry) was omitted revealed no positive signal. All antibodies, immunogen specificities, and chemicals used in these procedures are summarized in Table 2.

Data analysis

Standard light microscopy in combination with unbiased stereological techniques was used to estimate the age-related changes in $NADPHd^+$ and PV^+ cells of the SOC. With a projection microscope, anatomical borders were identified as regions of interest (ROI) and drawn on a grid. The area and volume of each section were then estimated by using the Cavalieri principle (Howard and Reed, 2005) such that:

$$A_{ref}=A/P \cdot \sum P$$

and

$$V_{ref}=A_{ref} \cdot T,$$

where A/P is the area between adjacent points on the grid, ΣP is the sum of all points within the ROI, and T is the tissue thickness. ROIs were drawn by one observer, but the cell counts were performed by two separate observers. All observers were blind to age.

To account for variations in tissue thickness from histological processing, an optical fractionation approach was used to estimate the number of positively labeled neurons (Mounton, 2002). This procedure eliminates bias produced by changes in the reference space. By using an optical disector, estimated cell numbers (E_n) were calculated as follows:

$$E_n=N_v \cdot V_{ref}$$

where

$$N_v=\sum Q/(n \cdot V_{dis})$$

and where N_v represents the points counted in the volume, V_{ref} is the volume calculated by the Cavalieri principle, Q is the number of cells counted, n is the number of disectors (sections counted), and V_{dis} is the volume of each disector. Because N_v and V_{ref} refer to a common volume, the total number of objects is estimated while controlling for volume changes. Previous studies have shown that calculations are most accurate when one-fourth to one-fifth of the average cell height is used as a guard space on either side of the z-plane of the disector (Mounton, 2002). One-fourth of a cell height was used in the present study, and the average cell heights used were 14.35 μm in the MNTB, 13.35 lm in the MSO, and 17.17 lm in the LSO (Bazwinsky et al., 2005).

Because the SOC is small, every positively stained neuron was counted within each ROI by the two observers. A cell had to contain label and have a punctate, cellular-like morphology to be counted. The corrected counts were then divided by the estimated volume to get the estimated cell density per ROI. Interobserver agreement was over 95%, and a paired *t*-test revealed no differences between counters ($P > 0.3$). The density values used for analysis are the averages of both observers' estimates.

To investigate any topographic (corresponding to the tonotopic organization of the SOC) differences in the measured cell densities, we partitioned the MNTB and LSO into medial, central, and lateral segments and the MSO into dorsal, central, and ventral segments corresponding to the low-, middle-, and high-frequency representations of each nuclei

(Guinan et al., 1972; Casseday et al., 1988; Kelly et al., 1998; Kandler et al., 2009). This volume partition was accomplished by grouping one-third of each ROI's counted points into the medial, central, and lateral sections or the dorsal, central, and ventral section. Cells in each one-third were then counted with the same criteria as in the total nucleus density estimation; however, cells touching the drawn borders between these regions were excluded from density calculations to limit counting biases between regions.

To ensure the observer's ability to differentiate positively labeled soma from the background staining of the neuropil reliably, a subset of sections from each of the three nuclei was further analyzed. A sample was randomly chosen, and cells were counted according to the methods and criteria described above. Images were then taken at several planes (three to five images per sample) of each section, spanning the height of the disector. The images were converted to black and white, thresholded, and binarized in Adobe Photoshop CS5 such that values of 1 (black) consisted of the lowest intensity value corresponding to a counted cell (measured and set by one observer), and the rest of the image was given a value of 0 (white). Another observer counted the black points with the size and shape of the soma counted in the real tissue (for which counters were over 95% in agreement). The result of this analysis showed that the observers reliably differentiated labeled cells from background staining in the neuropil (see Results).

Statistical analysis

Statistical analysis was performed in three steps using SPSS version 19 (SPSS, Chicago, IL). First, the animals were categorized as middle aged or old, with 22 (roughly 65 human years) as the cutoff age. There were four animals per group, and their density values were compared by using an unpaired t-test with a significance criterion of $P < 0.01$. Second, ABR–density relationships were analyzed by finding the Pearson product moment correlation along with a Monte Carlo analysis. This analysis was performed by randomly reassigning all of the ABR amplitudes to new density values and finding the R value of this random relationship. This procedure was repeated 1,000 times, and the *P* value obtained is the percentage of times that the random relationship gave an R value greater than or equal to the observed R value. Therefore the Monte Carlo provides the probability that the observed correlation is due to chance. To ensure validity further, given the relatively small sample, ABR–density relationships were considered significant only if the $P < 0.05$ by the Monte Carlo (i.e., a regression coefficient was greater than 950/1,000 coefficients generated by chance) and the R^2 value exceeded 0.35.

Results

Distribution of the NOS NADPHd and the calcium-binding protein PV in the SOC

We examined the SOC in histological sections collected from eight rhesus macaques ranging in age from 12 to 35 years. In all monkeys, the MSO and the MNTB had positive reactivity for both the NO synthase NADPHd and the calcium-binding protein PV. In one animal, there was no NADPHd staining in the LSO on either side of the midline, although good staining was seen in the other seven monkeys. Figure 1 shows an example of a transverse section through the SOC stained for NADPHd obtained from a 15-year-old

animal. The three primary subdivisions were defined following the conventions of Strominger and Hurwitz (1976) and Irving and Harrison (1967). The MSO was characterized by a slender, vertically oriented cell-rich region in the caudal pontine tegmentum surrounded by a clear zone of neuropil. A globular cell-rich region located lateral and slightly dorsal to the MSO characterized the LSO, and the MNTB was identified as a cell-rich region with large perikarya lying medial and ventral to the MSO. Figure 1 shows the SOC with the three principle subdivisions labeled for clarity and is representative of our sample in that the density of $NADPHd^+$ cells varied among the three subdivisions. Similar results were seen for PV^+ sections.

In rodents, cats, and echolocating bats, the MNTB, MSO, and LSO are tonotopically organized from medial to lateral (MNTB and LSO) or from dorsal to ventral (MSO; Guinan et al., 1972; Casseday et al., 1988; Kelly et al., 1998; Kandler et al., 2009). Although to our knowledge a similar organization has not been demonstrated there, the primate brain is likely to have a similar organization. Therefore, at the first level of analysis, we investigated whether location (frequency)-specific changes in immunoreactive cell densities existed as a function of age. We compared the relative density of both cell types in each subdivision after dividing the volume into one-thirds, corresponding to the low-, middle-, and high-frequency representations. The MNTB and LSO were partitioned into medial, central, and lateral segments, whereas the MSO was partitioned into dorsal, central, and ventral sections (see Materials and Methods). This analysis revealed no differences between partitions within the same animal (paired *t*-test, $P > 0.05$), particularly between the two extremes (i.e., medial vs. lateral and dorsal vs. ventral). Additionally, changes between animals were constant throughout the nuclei; i.e., no partition in any subdivision of the SOC changed to a greater extent than any other with age. Therefore, positively stained cells were uniformly distributed throughout the different subdivisions of the SOC regardless of age or presumed frequency representation. We therefore combined these three partitions for all subsequent analysis.

Age-related changes in the expression of $NADPHd^+$ and PV^+ cells

The primary objective of this study was to determine whether there are any age-related changes in the density of $NADPHd^+$ and PV^+ cells within the primate SOC. Figure 2 shows representative examples of the three subdivisions stained for NADPHd from a young monkey (15 years; Fig. 2A,C,E) and our oldest animal (35 years; Fig. 2B,D,F). It is apparent from these examples that the older animal had a greater density of $NADPHd^+$ neurons compared with the younger animal in the MSO (compare Fig. 2C and D). This difference is not as apparent from these examples for the MNTB or LSO (compare Fig. 2A with B and E with F). Figure 3 shows the adjacent sections from the same animals stained for PV immunohistochemistry. Again, these sections show an increase in PV^+ neurons in the MSO (compare Fig. 3C and D) that is not as apparent in the MNTB or LSO (compare Fig. 3A with B and E with F). This general finding was consistent throughout the different sections of the SOC analyzed from the eight monkeys.

Dense neuropilar staining was noted in the MSO and LSO but to a much lesser extent in the MNTB (Figs. 1-3). To ensure that our observers could reliably distinguish labeled cells from the background staining, we performed a threshold analysis on digitized images of the three

subdivisions (see Materials and Methods; Fig. 4A). The MNTB served as a control in these comparisons because of its noticeably reduced background staining compared with the MSO and LSO (Figs. 1–3). Figure 4A shows a sample at two planes of section from the LSO in its original form (top) and the same images after digitization and thresholding (bottom). This particular example has relatively high background staining compared with the rest of our data set. Note that, as the plane moved, the observer could reliably count cells that were unclear at other planes of the disector. Each sample was sectioned in three to five planes (depending on the tissue thickness) for this analysis. The observer's density calculations and the density calculations from the threshold images were significantly correlated in the MNTB and in the MSO/LSO for NADPHd ($r = 0.984$, $P < 0.001$; $r = 0.932$, $P < 0.001$, for the MNTB and MSO/LSO, respectively; Fig. 4B) and PV ($r = 0.959$, $P < 0.001$; $r = 0.900$, $P < 0.001$, for the MNTB and MSO/LSO, respectively; Fig. 4C). Furthermore, the 95% confidence interval for all sets of data encompassed the unity line (slope 1, intercept 0) in all cases for NADPHd- and PV-stained sections. Taken together, these results confirm that the observers' reliably differentiated positively labeled cells from background staining in the MSO and LSO.

Our qualitative impressions (Figs. 2, 3) were then tested quantitatively. All positively labeled cells were counted within the MNTB, MSO, and LSO of each animal, and the densities were calculated (see Materials and Methods). Animals were classified as middle-aged (12, 15, 15, and 20 years; roughly 37–61 human years) or old (22, 23, 27, and 35; roughly 67–107 human years) and compared. This analysis revealed that age-related changes within the MNTB, MSO, and LSO were similar for $NADPHd^+$ and PV^+ cell expression. $NADPHd^+$ cell density showed no changes with age in the MNTB or LSO (unpaired *t*-test $P > 0.05$; Fig. 5A) but significant increases in the aged MSO (unpaired *t*-test $P < 0.01$; Fig. 5A). Age-related changes of PV expression followed the same pattern, in which the MNTB and LSO showed no changes in density with age (unpaired *t*-test $P > 0.05$; Fig. 5B), but the MSO significantly increased its expression of PV^+ cells (unpaired *t*-test $P < 0.01$; Fig. 5B). Moreover, there was a significant correlation between the densities of the two cell types and age in the MSO, accounting for approximately 50% of the variance in this measure ($r = 0.77$, $P < 0.05$). These results demonstrate that changes in $NADPHd^+$ or PV^+ cell expression within the SOC are not the result of general differences of the aging nervous system (for example, differences in vascularization, permeability of the individual cells to the histochemical processes, or differences in immunoreactivity as a function of age). Rather, the changes are specific to the MSO, because no significant correlations were seen in the MNTB or LSO.

Macaque ABRs change with age

ABR recordings were collected from all monkeys with the exception of the youngest animal (147 months; see Materials and Methods and Table 1). Stimuli consisted of clicks, low-frequency tones (0.5, 1.0, and 2.0 kHz), middle-frequency tones (4.0 and 8.0 kHz), and high-frequency tones (12.0 and 16.0 kHz).

Figure 6A shows reconstructed ABR waveforms to clicks from a 15-year-old animal at different stimulus intensities. Peaks II and IV are labeled when present and were the most

salient early waveforms across all animals. For this animal, clear peaks II and IV were seen at the highest intensity presented, and these peaks decreased in amplitude and increased in latency as the stimulus intensity decreased. Note that stimuli 30 dB SPL and quieter did not evoke either a peak II or a peak IV. All animals showed similar decreases in amplitude and increases in latency as a function of decreasing stimulus intensity, with all stimulus types presented.

ABR amplitudes and immunopositive cell densities correlate in the MSO

When considering the ascending auditory pathway, anatomically the SOC is presumed to lie after the origin point of peak II and before the origin point of peak IV of the macaque ABR and likely contributes to both waveforms (Møller and Burgess, 1986). Our motivation was to determine whether hearing ability was correlated with $NADPHd^+$ and PV^+ cell densities independent of chronological age. Previous studies have shown that there are positive correlations between age and ABR thresholds in macaques (Navarro et al., 2008; Fowler et al., 2010); however, there was considerable variability across individuals in those studies. Given our relatively small sample, we found a modest and nonsignificant regression coefficient of 0.36 (Fig. 6B) between age and ABR thresholds from all stimulus types. To investigate the degree of correlation between $NADPHd^+$ and PV^+ cell density with both peaks of the ABR, regression analyses were conducted between cell density and the amplitude and the latency of each peak. This analysis used two different stimulus intensities for the clicks, low-, middle-, and high-frequency tones. The first intensity tested was 70 dB SPL, which was a suprathreshold stimulus eliciting identifiable peaks II and IV in all animals with the exception of the 35-year-old animal for some stimuli. The second intensity tested was the ABR threshold, which we defined as the last intensity evoking both peaks II and IV of the ABR.

The results of this analysis showed that the latencies of peak II or peak IV did not correlate with cell densities of either stain in any subdivision of the SOC at either 70 dB or threshold intensities. Furthermore, regression analyses revealed no significant correlations between either $NADPHd^+$ or PV^+ densities in any SOC subdivision and wave II or wave IV amplitudes when low-frequency stimuli of any intensity were used. Similarly, amplitudes from middle- and high-frequency tones at 70 dB or threshold showed no significant correlations with MNTB or the LSO densities (all $P > 0.05$). However, MSO densities showed significant correlations with ABR peaks in some but not all comparisons (Figs. 7, 8), as described below.

In the MSO, when 70 dB SPL stimuli were used, there was a significant correlation between peak II amplitudes from high-frequency tones and $NADPHd^+$ densities ($r = -20.609$, $P < 0.05$; Fig. 7B) but not with PV^+ densities (Fig. 7E,F). Furthermore, peak IV amplitudes from middle frequencies were significantly correlated with both $NADPHd^+$ and PV^+ cells ($r = -20.871$, $P < 0.05$ [Fig. 7C] and $r = -20.817$, $P < 0.05$ [Fig. 7G], respectively). High-frequency peak IV amplitudes were also negatively correlated with $NADPHd^+$ densities ($r = -20.599$, $P < 0.05$; Fig. 7D), but this correlation did not reach significance with PV+ densities by our criteria of a stringent R^2 value ($r = -20.522$, $P < 0.05$, $r^2 < 0.35$; Fig. 7H).

Threshold stimuli produced effects in the MSO similar to those seen at 70 dB (Fig. 8). Similar to the findings with the higher intensity stimuli, peak II evoked by high-frequency tones was significantly correlated with $NADPHd^+$ densities ($r = -20.642$, $P < 0.05$; Fig. 8B), and PV^+ densities showed a nonsignificant trend ($r = -20.506$, $P < 0.05$, $r^2 < 0.35$; Fig. 8F). Peak IV amplitudes to middle-frequency tones did not establish significant trends with cell density (Fig. 8C,G), but with high-frequency tones there were significant negative correlations between peak IV and both $NADPHd^+$ ($r = -20.726$, $P < 0.05$; Fig. 8D) and PV^+ ($r = -20.644$, $P < 0.05$; Fig. 8H).

To summarize, consistent with the analysis of cell density as a function of age, only the MSO cell densities were correlated with the ABR amplitudes of peaks II and IV. These comparisons revealed negative correlations between cell densities and ABR amplitudes that reached significance only with high- and middle-frequency tones. Taken together, these results demonstrate that age-related changes in the properties of ABRs correlated with $NADPHd^+$ and PV^+ cell density, but only within specific subdivisions. Interestingly, the MSO is tuned to lower frequencies, but its cell densities correlate with ABR amplitudes only at the higher end of the frequency spectrum.

Click stimuli and tone stimuli show opposite trends

To investigate how $NADPHd^+$ and PV^+ densities correlate with ABR responses to click stimuli, we combined the cell densities of the MNTB, MSO, and LSO (see Materials and Methods), reasoning that all three subdivisions participate in the generation of the ABR response to this broad-spectrum stimulus. In addition, many nonsignificant trends emerged in our analysis separating each nucleus; therefore, combining all subdivisions of the SOC could reveal statistically significant correlations. We also reanalyzed the low-, middle-, and high-frequency tone data after combining the positively labeled cell densities across the three subdivisions in the same manner. This analysis revealed no significant correlations between cell densities and peak II amplitudes at any intensity, or peak II or peak IV amplitudes, using 70 dB SPL stimuli (all $P > 0.05$; data not shown). For threshold stimuli, however, peak IV amplitudes to click stimuli positively and significantly correlated with both $NADPHd^+$ ($r = 0.838$, $P < 0.01$) and PV^+ ($r = 0.729$, $P < 0.05$) cell densities (Fig. 9). The results for the tone stimuli showed very different trends, however. There was a negative correlation between wave IV amplitudes from high-frequency stimuli presented at threshold with cell densities using both stains (Fig. 9B), although with more modest correlation coefficients than were seen with click stimuli ($r = -20.552$, $P < 0.05$; $r = -20.599$, $P < 0.05$, for $NADPHd^+$ and PV^+, respectively; Fig. 9B). The correlations between the low- and middle-frequency tones with either stain did not reach statistical significance (Fig. 9C,D), suggesting that the trends seen with tones are driven by the changes in cell density of the MSO described earlier (Fig. 8).

These results led us to investigate the differences between click responses and tone responses near threshold. Upon visual inspection of the ABRs, we noticed that click amplitudes sharply decreased in magnitude at intensity levels leading down to threshold, whereas tone amplitudes remained fairly constant around these intensities (i.e., there appeared to be a faster drop in ABR amplitudes to click stimuli), especially in aged animals.

To quantify these observations, we compared the difference in the magnitude of the evoked potentials between the peak IV amplitude 10 dB SPL above threshold and that at threshold for both tone and click stimuli. Larger values indicate that the amplitude difference between these two intensities was greater, so they indicate a steeper drop. Results indicate that clicks produced the greatest (and the only significant) amplitude differences between these two intensity levels. Furthermore, this amplitude difference was observed only in old monkeys (Fig. 10A), indicating a steeper drop in the response to clicks with age. There were no age-related differences seen for any tone value. These amplitude differences to click stimuli showed weak, yet insignificant, correlations with the cell densities of the MNTB (r = 0.187, $P = 0.07$; r = 0.210, $P = 0.09$, for NADPHd and PV, respectively), MSO (r = 0.296, $P = 0.06$; r = 0.276, $P = 0.075$, for NADPHd and PV, respectively), and LSO (r = 0.114, $P = 0.12$; r = 0.178, $P = 0.10$, for NADPHd and PV, respectively). However, these values reached significance when correlated with cell densities of the combined SOC (r = 0.685, $P < 0.05$; r = 0.670, $P < 0.05$, for NADPHd and PV, respectively; Fig. 10B). Although correlative, these observations suggest that the cell density changes seen in older monkeys play a role in the different response properties of the brainstem to clicks and tones.

We also noted that the wave IV amplitudes were generally greater at threshold to click stimuli compared with tone stimuli. To test this observation, we performed regression analyses on the differences between the wave IV amplitudes to click and tone stimuli and cell densities. Larger values indicate a greater response amplitude to clicks than for tones at threshold (we did not see a similar effect at 70 dB SPL). These correlations were significant in the MNTB (r = 0.714, $P < 0.05$; r = 0.844, $P < 0.05$, for NADPHd and PV, respectively), MSO (r = 0.622, $P < 0.05$; r = 0.907, $P < 0.05$, for NADPHd and PV, respectively), and LSO (r = 0.820, $P < 0.05$; r = 0.741, $P < 0.05$, for NADPHd and PV, respectively), and the results after combining densities across the SOC subdivisions are shown in Figure 11A. These findings show that the differences between the response to clicks and tones are correlated with increases in cell density. Finally, we tested whether these differences between click and high-frequency tone amplitudes correlate better with age or with cell densities, and the results of this analysis are shown in Figure 11B. We found a strong correlation between age and the amplitude of peak IV evoked by click stimuli (r = 0.707, $P < 0.05$; Fig. 11B), but this correlation was not as strong as that seen between these amplitudes and the cell densities of the SOC (compare Fig. 11A and B).

Discussion

Functional consequences of age-related changes in the primate SOC

The major purpose of this study was to characterize the age-related neurochemical changes in NADPHd and PV reactivity in the macaque auditory brainstem. Despite several studies of this type in rodent models, there have been far fewer studies in macaques. We have seen that the macaque IC increases its PV expression while keeping NADPHd constant (unpublished observations), conflicting with rodent studies. The results for the SOC described here both agree and disagree with the rodent literature. In agreement is that $NADPHd^+$ cells increased in the SOC (Reuss et al., 2000). Our results differ from the rodent in that we observed an increase in PV^+ cells with age, in contrast to the decreases in several calcium-binding

proteins seen in rodent SOCs (Zettel et al., 1997). The rodent MNTB shows more anatomical changes than any of the other subdivisions of the SOC (Casey, 1990), which contradicts the current data, in which the MNTB showed the least change with age. Overall, there is considerable variability between different rodent studies, and our results for the macaque suggest that the age-related changes are different between primates and rodents, which together make generalizations between these two animal models troublesome.

$NADPHd^+$ and PV^+ cells are both active in neural signaling within the nervous system, but through distinctly different mechanisms. NADPHd produces NO, which diffuses from the cell, acting upon local cells containing the enzyme soluble guanylate cyclase (sGC), which is considered the primary physiological target of neuronal NO (Esplugues, 2009). sGC in turn increases the concentration of cyclic GMP (cGMP), facilitating several cellular processes by targeting phosphodiesterases (PDEs), kinases, and ion channels (Derbyshire and Marletta, 2012). As a signaling molecule, NO's initiation of this sGC-dependent biochemical cascade is considered its primary role in the nervous system, with no exception in the auditory system. Another compelling theory is that NO acts as a feedback inhibitor of glutamatergic N-methyl-D-aspartate (NMDA) receptors (glut-NMDArs). Support for this exists in the physical linkage of neural NO synthase proteins with glut-NMDArs and in NO's inhibition of the receptor's activity (Manzoni and Bockaert, 1993). This negative feedback could prevent saturation of neural responses during periods of high physiological activity.

The ability of neurons to phase lock precisely to auditory signals is critical for coincidence detection and ITD tuning (Batra et al., 1997; Fitzpatrick et al., 2000). Few studies have tested phase locking of neurons in aged brains, although those that have indicate that aged neurons show deficits in following fast temporal stimuli (see, e.g., Schatteman et al., 2008). Once the neural response is beyond single action potentials for each stimulus cycle, the phase-locking ability of neurons can be little affected by the overall firing rate of the neurons. In this case, inhibitory input with the appropriate timing could help to refine and tune the response, giving rise to higher firing rates to the peak of the response compared with the trough. One possibility is that, because NO inhibits glut-NMDArs, it may have a role in preserving phase locking of neurons in addition to initiating cGMP-dependent biochemical signaling and modulatory pathways. NADPHd changes were noted in the high-frequency-biased LSO (although not significantly) with age and within the MSO when correlated with higher frequency ABRs, especially at threshold. These results are consistent with either a role in high-frequency processing for NO in aged macaques or alternatively in maintaining constancy of low-frequency processing with age (discussed below).

PV^+ neurons have been well characterized in the cerebral cortex, but in the brainstem the role of these neurons is not nearly as well understood. In the neocortex, PV^+ cells are one of the three major interneuron types and account for roughly 40% of all cortical interneurons (Rudy et al., 2011). These GABA-releasing neurons have fast spiking physiological response properties that produce high-frequency trains of brief action potentials with little spike frequency adaptation (Kawaguchi et al., 1987; Cauli et al., 1997; Kawaguchi and Kubota, 1997; Gibson et al., 1999; Ascoli et al., 2008; Xu and Call-away, 2009). At subcortical levels, however, there is evidence indicating that both inhibitory and excitatory cells can be PV positive. Colocalization studies show that at various levels of the rodent

auditory brainstem, including the SOC, PV does not colocalize with GABA or glycine but rather colocalizes with glutamate (Fredrich and Reisch, 2009). This observation suggests that PV's role in the SOC is not analogous to its role in cortex, and further studies investigating the physiology and chemistry of PV^+ cells at this level of the nervous system are necessary to understand the role of subcortical PV^+ neurons. Nevertheless, whether excitatory or inhibitory, PV^+ cells likely play a modulatory role in the SOC necessary for the preservation of some function, because age-related changes have now been noted in multiple species

MSO shows significant age-related increases of both NADPHd and PV

MNTB, MSO, and LSO all participate in sound source localization and are located within tens of micrometers from each other, yet only the MSO showed significant age-related changes in NADPHd and PV expression. There are at least three possibilities to explain the differences between these three subdivisions. First, a larger proportion of cells in the MSO is tuned to lower frequencies compared with the high-frequency-biased MNTB and LSO. The monkey audiogram shows the highest sensitivity to lower frequencies compared with higher frequencies, indicating that these frequencies likely carry more importance to the macaque (Recanzone, 2008). Thus, the neurochemical changes seen in the MSO could reflect a compensatory mechanism to preserve the low-frequency processing that degrades with age. This is consistent with finding that only high- and middle-frequency ABR amplitudes correlate with changes in $NADPHd^+$ density. Although it is tempting to think that ABR amplitudes directly correlate with the strength of the auditory signal, this does not necessarily have to be the case. The ABR sums the neural activity at any given time, so differences in ABR amplitudes may reflect greater or less temporal cohesion of neural information ascending the auditory system, not changes in the absolute spiking activity. The upregulation of NADPHd and PV may therefore help to maintain the proper temporal fidelity of the responses to low-frequency stimuli. The result of this maintenance would be reflected by consistent ABR amplitudes to these low-frequency stimuli across age groups. As noted above, lower frequencies are more behaviorally and physiologically important to the macaque, and aged macaques have a greater need for lower frequency processing compared with high-frequency processing. Thus, changes in NADPHd and PV density could function to keep the neural response properties to low frequencies as constant as possible with age, at the expense of high-frequency processing.

The alternative to this view is that these proteins reflect neural dysfunction, indicating that the MSO deteriorates to a greater extent with age compared with other SOC subdivisions, with the higher frequencies showing the greatest deterioration. This possibility predicts that aged primates would show sound localization deficits that are selective for middle-frequency stimuli at the high-frequency end of the effectiveness of ITD and IPD binaural cues. This is consistent with the observation that human subjects show localization deficits at the high-frequency end of the effective ITD/IPD range (1,250–1,575 kHz) that do not occur at the lower end (Dobreva et al., 2011). Furthermore, the upper frequency limit for processing of temporal cues also declines with age (Grose and Mamo, 2010). Our data suggest that, within the MSO, some of these processing deficits seem to be accompanied by neurochemical changes. Whether these neurochemical changes protect low-frequency responses or are

partially responsible for the declines observed at the higher frequency end of the effective range cannot be determined from these data.

A third alternative is that the high-frequency tones elicit a smaller overall response in older animals (with or without changes in the temporal fidelity). This is consistent with age-related changes in the macaque cochlea, in which histopathologies are seen to the greatest extent in the basal turn (high-frequency zone) of the inner ear (Engle and Recanzone, 2012). Specifically, hair cell and spiral ganglion cell loss is most prominent in this region of the cochlea. Thus, with fewer transducing cells dedicated to high-frequency processing, the signal in the central auditory system would likely be reduced. If this is the case, then the chemical changes described for the MSO may be unrelated to ABR amplitudes, and the correlations that were seen instead may reflect some noncausal mechanisms.

The MNTB did not change its expression of any cell type

The MSO showed significant age-related changes in $NADPHd^+$ and PV^+ cell density, and the LSO showed nonsignificant trends, but the MNTB did not alter its expression of either cell type as a function of age or ABR. The large principle cells of the MNTB show many fundamental chemical differences from the smaller excitatory cells of the MSO and LSO. Glycine is especially prominent in the MNTB compared with the MSO and LSO (Smith et al., 1998). However, the functional implications of these chemical differences are unclear, but they do suggest that the subregions of the SOC should not be viewed as chemically analogous. Our results could reflect age-related differences in NADPHd and PV expression characteristic of different chemically defined cell classes in the SOC. Regardless of the reason behind the observed lack of change in the MNTB, this constancy served as a powerful control to the changes seen in the MSO, because both subdivisions were observed in the same sections.

Click ABRs and tone ABRs behave oppositely at wave IV with age

We found that wave IV showed an age-related decrease in amplitude in response to tones but also a surprising increase in amplitude in response to clicks. This finding suggests a shift in the way in which these stimuli are processed in older macaques. Given that these changes were also correlated with both $NADPHd^+$ and PV^+ cell density, these cells could contribute to this observation. Our regression analyses indicated that the cell density is a better predictor than age in explaining the differences in the response amplitudes to clicks over tones. However, other age-related changes of the auditory system certainly play a role in these observations. For example, changes in the net input, spike timing, and GABAergic and glycinergic local inhibition would all change the way in which these stimuli are processed. These changes are reflected only broadly in the ABR, and the underlying mechanisms cannot be teased apart with the current data.

The temporal fidelity of the neural response (as discussed above) produced by each stimulus might also explain the difference between the responses to clicks over tones in the ABR. If clicks elicit a discharge of action potentials arriving at the SOC with more cohesion compared with tone-elicited spikes, then the ABR amplitudes would appear larger even if the same total numbers of action potentials were fired. Depending on the physiology of PV^+

and NADPHd$^+$ cells in the SOC, higher (or lower) cell densities could exaggerate this difference in the ABR. Unfortunately, as noted above, the physiology of these cell types remains unclear. When considering ABR thresholds, it is also important to keep in mind that there are sex differences in the ABR in that female primates tend to show shorter latencies than males (Patterson et al., 1981), suggesting slight differences in auditory processing. The animals used in the current study were both male and female, with females making up a greater proportion of the aged group (see Table 1).

Summary

The results of this study indicate that NADPHd and PV expression increases in the SOC of normally aging nonhuman primates. Correlations between these changes in density and changes in ABRs demonstrated that amplitudes increase as NADPHd density decreases. Curiously, amplitudes to click stimuli behaved in the opposite pattern compared with those evoked by tone stimuli as a function of age, implying a shift in the way aged primates process the two stimuli. Our regression model indicated that cell density was a better predictor than age for all amplitude changes. We interpret these results to mean that PV$^+$ and NADPHd$^+$ cells contribute significantly to age-related changes in the macaque ABR in particular and in auditory processing in general.

Acknowledgments

The authors thank Xochi Navarro, Dina Juarez-Salinas, Anastasiya Petrovska, and Marianthi Gelatos for their help with this project and Rhonda Oates-O'Brien and Guy Martin for excellent animal care.

Grant sponsor: National Institute on Aging; Grant number: R21AG024372 (to G.H.R.); Grant number: R01AG034137 (to G.H.R.); Grant sponsor: National Institute of Deafness and Other Cummunication Disorders; Grant number: T32DC008072 (to J.R.E.).

Literature Cited

Allen AR, Starr A. Auditory brain stem potentials in monkey (*M. mulatta*) and man. Electroencephalogr Clin Neurophysiol. 1978; 45:53–63. [PubMed: 78822]

Ascoli GA, Alonso-Nanclares L, Anderson SA, Barrionuevo G, Benavides-Piccione R, Burkhalter A, Buzsaki G, et al. Petilla terminology: nomenclature of features of GABAergic interneurons of the cerebral cortex. Nat Rev. 2008; 9:557–568.

Bartos M, Elgueata C. Functional characteristics of parvalbumin- and cholecystokinin-expressing basket cells. J Physiol. 2012; 590:669–681. [PubMed: 22250212]

Batra R, Kuwada S, Fitzpatrick DC. Sensitivity to inter-aural temporal disparities of low and high frequency neurons in the superior olivary complex. II. Coincidence detection. J Neurophysiol. 1997; 78:1237–1247. [PubMed: 9310415]

Bazwinsky I, Bidmon HJ, Zilles K, Hilbig H. Characterization of the rhesus monkey superior olivary complex by calcium binding proteins and synaptophysin. J Anat. 2005; 207:745–761. [PubMed: 16367802]

Bon CL, Garthwaite J. Exogenous nitric oxide causes potentiaon of hippocampal synaptic transmission during low-frequency stimulation via the endogenous nitric oxide-cGMP pathway. Eur J Neurosci. 2001; 14:585–594. [PubMed: 11556884]

Bon CL, Garthwaite J. On the role of nitric oxide in hippocampal long-term potentiation. J Neurosci. 2003; 23:1941–1948. [PubMed: 12629199]

Boudreau JC, Tsuchitani C. Binaural interaction in the cat superior olive S segment. J Neurophysiol. 1968; 31:442–454. [PubMed: 5687764]

Brand A, Behrend O, Marquardt T, McAlpine D, Grothe B. Precise inhibition is essential for microsecond interaural time difference coding. Nature. 2002; 417:543–547. [PubMed: 12037566]

Bredt DS, Snyder SH. Isolation of nitric oxide synthetase, a calmodulin-requiring enzyme. Proc Natl Acad Sci U S A. 1990; 87:682–685. [PubMed: 1689048]

Bredt DS, Glatt CE, Hwang PM, Fotuhi M, Dawson TM, Snyder SH. Nitric oxide synthase protein and mRNA are discretely localized in neuronal populations of the mammalian CNS together with NADPH diaphorase. Neuron. 1991; 7:615–624. [PubMed: 1718335]

Brenman JE, Chao DS, Gee SH, McGee AW, Craven SE, Santillano DR, Wu Z, Huang F, Xia H, Peters MF, Froehner SC, Bredt DS. Interaction of nitric oxide synthase with the postsynaptic density protein PSD-95 and alpha1-syntrophin mediated by PDZ domains. Cell. 1996; 84:757–767. [PubMed: 8625413]

Carder RK, Leclerc SS, Hendry SH. Regulation of calcium-binding protein immunoreactivity in GABA neurons of macaque primary visual cortex. Cereb Cortex. 1996; 2:271–287. [PubMed: 8670656]

Casey MA. The effects of aging on neuron number in the rat superior olivary complex. Neurobiol Aging. 1990; 11:391–394. [PubMed: 2381498]

Caspary DM, Milbrandt JC, Helfert RH. Central auditory aging: GABA changes in the inferior colliculus. Exp Gerontol. 1995; 30:349–360. [PubMed: 7556513]

Caspary DM, Holder TM, Hughes LF, Milbrandt JC, McKernan RM, Naritoku DK. Age-related changes in $GABA_A$ receptor subunit composition and function in rat auditory system. Neuroscience. 1999; 93:307–312. [PubMed: 10430494]

Caspary DM, Schatteman TA, Hughes LF. Age-related changes in the inhibitory response properties of dorsal cochlear nucleus output neurons: role of inhibitory inputs. J Neurosci. 2005; 25:10952–10959. [PubMed: 16306408]

Caspary DM, Hughes LF, Schatteman TA, Turner JG. Age-related changes in the response properties of cartwheel cells in rat dorsal cochlear nucleus. Hearing Res. 2006; 216/217:207–215.

Caspary DM, Ling L, Turner JG, Hughes LF. Inhibitory neurotransmission, plasticity and aging in the mammalian central auditory system. J Exp Biol. 2008; 211:1781–1791. [PubMed: 18490394]

Casseday JH, Covey E, Vater M. Connections of the superior olivary complex in the rofous horshoe bat *Rhinolophus rouxi*. J Comp Neurol. 1988; 278:313–329. [PubMed: 2464005]

Cauli B, Audinat E, Lambolez B, Angulo MC, Ropert N, Tsuzuki K, Hestrin S, et al. Molecular and physiological diversity of cortical nonpyramidal cells. J Neurosci. 1997; 17:3894–3906. [PubMed: 9133407]

Davis, RT.; Leathers, CW. Behavior and pathology of aging in rhesus monkeys. New York: Alan R. Liss, Inc; 1985.

Dawson TM, Bredt DS, Fotuhi M, Hwang PM, Snyder SH. Nitric oxide synthase and neuronal NADPH diaphorase are identical in brain and peripheral tissues. Proc Natl Acad Sci U S A. 1991a; 88:7797–7801. [PubMed: 1715581]

Dawson VL, Dawson TM, London ED, Bredt DS, Snyder SH. Nitric oxide mediates glutamate neurotoxicity in primary cortical cultures. Proc Natl Acad Sci U S A. 1991b; 88:6368–6371. [PubMed: 1648740]

de la Mothe LA, Blumell S, Kajikawa Y, Hackett TA. Cortical connections of the auditory cortex in marmoset monkeys: core and medial belt regions. J Comp Neurol. 2006a; 496:27–71. [PubMed: 16528722]

de la Mothe LA, Blumell S, Kajikawa Y, Hackett TA. Thalamic connections of the auditory cortex in marmoset monkeys: core and medial belt regions. J Comp Neurol. 2006b; 496:72–96. [PubMed: 16528728]

Derbyshire ER, Marletta MA. Structure and regulation of soluble guanylate cyclase. Annu Rev Biochem. 2012; 81:533–559. [PubMed: 22404633]

Disterhoft JF, Moyer JR Jr, Thomson LT. The calcium rationale in aging and Alzheimer's disease. Evidence from an animal model of normal aging. Ann N Y Acad Sci. 1995; 747:382–406. [PubMed: 7847686]

Dobreva MS, O'Neill WE, Paige GD. Influence of aging on human sound localization. J Neurophysiol. 2011; 105:2471–2486. [PubMed: 21368004]

Engle JR, Recanzone GH. Characterizing spatial tuning functions of neurons in the auditory cortex of young and aged monkeys: a new perspective on old data. Front Aging Res. 2012; 4:36.

Engle JR, Tinling S, Recanzone GH. Age-related hearing loss in rhesus monkeys is correlated with cochlear histopathologies. PLoS One. 2013; 8:e550902.

Esplugues JV. NO as a signalling molecule in the nervous system. Br J Pharmacol. 2002; 135:1079–1095. [PubMed: 11877313]

Fessenden JD, Schacht J. The nitric oxide/cyclic GMP pathway: a potential major regulator of cochlear physiology. Hearing Res. 1998; 118:168–176.

Fitzpatrick DC, Kuwada S, Batra R. Neural sensitivity to interaural time differences: beyond the Jeffress model. J Neurosci. 2000; 20:1605–1615. [PubMed: 10662850]

Fowler CG, Chiasson KB, Leslie TH, Thomas D, Beasley TM, Kemnitz JW, Weindruch R. Auditory function in rhesus monkeys: effects of aging and caloric restriction in the Wisconsin monkeys five years later. Hearing Res. 2010; 261:75–81.

Fredrich M, Reisch A. Neuronal subtype identity in the rat auditory brainstem as defined by molecular profile and axonal projection. Exp Brain Res. 2009; 195:241–260. [PubMed: 19340418]

Galambos R, Schwartzkopf J, Rupert A. Microelectrode studyof superior olivary nuclei. Am J Physiol. 1959; 197:527–536. [PubMed: 13826000]

Gibson JR, Beierlein M, Connors BW. Two networks of electrically coupled inhibitory neurons in neocortex. Nature. 1999; 402:75–79. [PubMed: 10573419]

Grose JH, Mamo SK. Processing of temporal fine structure as a function of age. Ear Hear. 2010; 31:755–760. [PubMed: 20592614]

Guinan JJ, Norris BE, Guinan SS. Single auditory units in thesuperior olivary complex. II. Locations of unit categories and tonotopic organization. Int J Neurosci. 1972; 4:147–166.

Hackett TA, Preuss TM, Kaas JH. Architectonic identification of the core region in auditory cortex of macaques, chimpanzees, and humans. J Comp Neurol. 2001; 441:197–222. [PubMed: 11745645]

Hopper R, Lancaster B, Garthwaite J. On the regulation of NMDA receptors by nitric oxide. Eur J Neurosci. 2004; 19:1675–1682. [PubMed: 15078541]

Howard, V.; Reed, MG. Unbiased stereology: three-dimensional measurements in microscopy. 2nd. New York: Abingdon; 2005.

Huh Y, Choon Park D, Geun Yeo S, Cha C II. Evidence for increased NADPH-diaphorse-positive neurons in the central auditory system of the aged rat. Acta Otolaryngol. 2008; 128:648–653. [PubMed: 18568499]

Irving R, Harrison JM. The superior olivary complex and audition: a comparitive study. J Comp Neurol. 1967; 130:77–86. [PubMed: 4962091]

Jeffress LA. A place theory of sound localization. J Comp Physiol Psychol. 1948; 41:35–39. [PubMed: 18904764]

Juarez-Salinas DL, Engle JR, Navarro XO, Recanzone GH. Hierarchical and serial processing in the spatial auditory cortical pathway is degraded by natural aging. J Neurosci. 2010; 30:14795–14804. [PubMed: 21048138]

Kandler K, Clause A, Noh J. Tonotopic reorganization of the developing auditory brainstem circuits. Nat Neurosci. 2009; 12:711–717. [PubMed: 19471270]

Kawaguchi Y, Kubota Y. GABAergic cell subtypes and their synaptic connections in rat frontal cortex. Cereb Cortex. 1997; 7:476–486. [PubMed: 9276173]

Kawaguchi Y, Katsumaru H, Hosaka T, Heizmann CW, Hama K. Fast spiking cells in rat hippocampus (CA1 region) contain the calcium-binding protein parvalbumin. Brain Res. 1987; 416:369–374. [PubMed: 3304536]

Kelly JB, Liscum A, Van Adel B, Ito M. Projections from the superior olive and lateral leminiscus to tonotopic regions of the rat inferior colliculus. Hearing Res. 1998; 116:43–54.

Klausberger T, Somogyi P. Neuronal diversity and temporal dynamics: the unity of hippocampal circuit operations. Science. 2008; 321:53–57. [PubMed: 18599766]

Kulesza RJ Jr, Kadner A, Berrebi AS. Distinct roles for glycine and GABA in shaping the Response properties of neurons in the superior paraolivary nucleus of the rat. J Neurophysiol. 2007; 97:1610–1620. [PubMed: 17122321]

Laughlin NK, Hartup BK, Lasky RE, Meier MM, Hecox KE. The development of auditory event related potentials in the rhesus monkey (*Macaca mulatta*). Dev Psychobiol. 1999; 34:37–56. [PubMed: 9919432]

Lee HJ, Wallani T, Mendelson JR. Temporal processing speed in the inferior colliculus of young and aged rats. Hearing Res. 2002; 174:64–74.

Manzoni O, Bockaert J. Nitric oxide synthase activity endogenously modulates NMDA receptors. J Neurochem. 1993; 61:368–370. [PubMed: 7685816]

Mendelson JR, Rickets C. Age-related temporal processing speed deterioration in auditory cortex. Hearing Res. 2001; 158:84–94.

Møller AR, Burgess J. Neural generators of the brain-stem auditory evoked potentials (BAEPs) in the rhesus monkey. Electroencephalogr Clin Neurophysiol. 1986; 65:361–372. [PubMed: 2427327]

Mounton, PR. Principles and practices of unbiased stereology. Baltimore: Johns Hopkins University Press; 2002.

Navarro X, Engle J, Fletcher M, Juarez-Salinas D, Recanzone GH. Age-related changes in the auditory brainstem response to tones and noise in macaque monkeys. Soc Neurosci Abstr. 2008; 34

Oliver DL. Ascending efferent projections of the superior olivary complex. Microsc Res Techniq. 2000; 51:355–363.

O'Neill WE, Zettel ML, Whittemore KR, Frisina RD. Calbindin D-28k immunoreactivity in the medial nucleus of the trapezoid body declines with age in C57BL/6, but not CBA/CaJ, mice. Hearing Res. 1997; 112:158–166.

Ouda L, Nwabueze-Ogbo FC, Druga R, Syka J. NADPH-diaphorase-positive neurons in the auditory cortex of young and old rats. Neuroreport. 2003; 14:363–366. [PubMed: 12634484]

Ouda L, Druga R, Syka J. Changes in parvalbumin immunoreactivity with aging in the central auditory system of the rat. Exp Gerontol. 2008; 43:782–789. [PubMed: 18486384]

Padberg J, Cerkevich C, Engle J, Rajan AT, Recanzone G, Kaas J, Krubitzer L. Thalamocortical connections of parietal somatosensory cortical fields in macaque monkeys are highly divergent and convergent. Cereb Cortex. 2009; 19:2038–2064. [PubMed: 19221145]

Palombi PS, Backoff DM, Caspary DM. Responses of young and aged rat inferior colliculus neurons to sinusoidally amplitude modulated stimuli. Hearing Res. 2001; 153:174–180.

Patterson JV, Michalewski HJ, Thompson LW, Bowman TE, Litzelman DK. Age and sex differences in the human auditory brainstem response. J Gerontol. 1981; 36:455–462. [PubMed: 7252079]

Recanzone GH. Representation of con-specific vocalizations in the core and belt areas of the auditory cortex in the alert macaque monkey. J Neurosci. 2008; 28:13184–13193. [PubMed: 19052209]

Reuss S. Introduction to the superior olivary complex. Microsc Res Techniq. 2000; 51:303–306.

Reuss S, Schaeffer DF, Laages MH, Riemann R. Evidence for increased nitric oxide production in the auditory brain stem of the aged dwarf hamster (*Phodopus sungorus*): an NADPH-diaphorase histochemical study. Mech Aging Dev. 2000; 112:125–134. [PubMed: 10690925]

Rudy B, Fishell G, Lee S, Hjerling-Leffler J. Three groups of interneurons account for nearly 100% of neocortical GABAergic neurons. Dev Neurobiol. 2011; 71:45–61. [PubMed: 21154909]

Sanchez-Zuriaga D, Marti-Gutierrez N, De La Cruz MA, Peris-Sanchis MR. Age-related changes of NADPH-diaphorase-positive neurons in the rat inferior colliculus and auditory cortex. Microsc Res Techniq. 2007; 70:1051–1059.

Schatteman TA, Hughes LF, Caspary DM. Aged-related loss of temporal processing: altered responses to amplitude modulated tones in rat dorsal cochlear nucleus. Neuroscience. 2008; 154:329–337. [PubMed: 18384967]

Scherer-Singler U, Vincent SR, Kimura H, McGeer EG. Demonstration of a unique population of neurons with NADPH-diaphorase histochemistry. J Neurosci Methods. 1983; 9:229–234. [PubMed: 6363828]

Schulte BA, Schmiedt RA. Lateral wall Na, K-ATPase and endonuclear potentials decline with age in quiet-reared gerbils. Hearing Res. 1992; 61:35–46.

Shibuki K, Okada D. Endogenous nitric oxide release required for long-term synaptic depression in the cerebellum. Nature. 1991; 349:326–328. [PubMed: 1702879]

Smith PH, Joris PX, Yin TCT. Anatomy and physiology of principal cells of the medial nucleus of the trapezoid body (MNTB) of the cat. J. Neurophysiol. 1998; 79:3127–42.

Spicer SS, Schulte BA. Spiral ligament pathology in quiet-aged gerbils. Hear Res. 2002; 172:172–185. [PubMed: 12361880]

Stapells DR. Threshold estimation by the tone-evoked auditory brainstem response: a literature meta-analysis. J Speech Lang Pathol Audiol. 2000; 24:74–83.

Strominger NL, Hurwitz JL. Anatomical aspects of the superior olivary complex. J Comp Neurol. 1976; 170:485–497.10.1002/cne.901700407 [PubMed: 826550]

Tang AH, Karson MA, Nagode DA, McIntosh JM, Uebele VN, Renger JJ, Klugmann M, Milner TA, Alger BE. Nerve terminal nicotinic acetylcholine receptors initiate quantal GABArelease from perisomatic interneurons by activating axonal T-type (Ca_V3) Ca2 channels and Ca2 release from stores. J Neurosci. 2011; 31:13546–13561. [PubMed: 21940446]

Toescu EC, Vreugdenhil M. Calcium and normal brain ageing. Cell Calcium. 2010; 42:158–164. [PubMed: 20045187]

Tollin DJ. The lateral superior olive: a functional role in sound source localization. Neuroscientist. 2003; 9:127–143. [PubMed: 12708617]

Torre P 3rd, Fowler CG. Age-related changes in auditory function of rhesus monkeys (*Macaca mulatta*). Hearing Res. 2000; 142:131–140.

Torre P 3rd, Mattison JA, Fowler CG, Lane MA, Roth GS, Ingram DK. Assessment of auditory function in rhesus monkeys (*Macaca mulatta*): effects of age and calorie restriction. Neurobiol Aging. 2004; 25:945–954. [PubMed: 15212848]

Udell J, Engle J, Navarro X, Recanzone GH. Age-related effects on NADPH-diaphorase-positive neurons in the macaque inferior colliculus. Soc Neursoci Abstr. 2008; 35

Webster, WR. Auditory system. In: Paxinos, G., editor. The rat nervous system. San Diego: Academic Press; 1995. p. 797-831.

Xu X, Callaway EM. Laminar specificity of functional input to distinct types of inhibitory cortical neurons. J Neurosci. 2009; 29:70–85. [PubMed: 19129386]

Yin TC, Chan JC. Interaural time sensitivity in medial superior olive of cat. J Neurophysiol. 1990; 64:465–488. [PubMed: 2213127]

Zettel ML, Frisina RD, Haider SE, O'Neill WE. Age-related changes in calbindin D-28k and calretinin immunoreactivity in the inferior colliculus of CBA/CaJ and C57Bl/6 mice. J Comp Neurol. 1997; 386:92–110. [PubMed: 9303527]

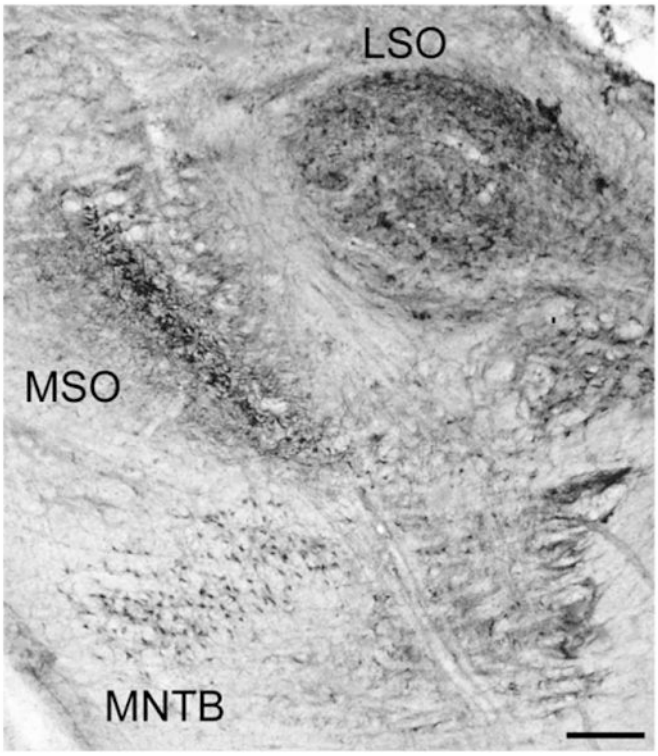

Figure 1.

Transverse NADPHd-stained section through the superior olivary complex (SOC). Labeled are the three subdivisions of the SOC: the medial nucleus of the trapezoid body (MNTB), medial superior olive (MSO), and lateral superior olive (LSO). The left side of this image corresponds to the medial aspect and the top to the dorsal aspect of the section. Scale bar = 500 μm.

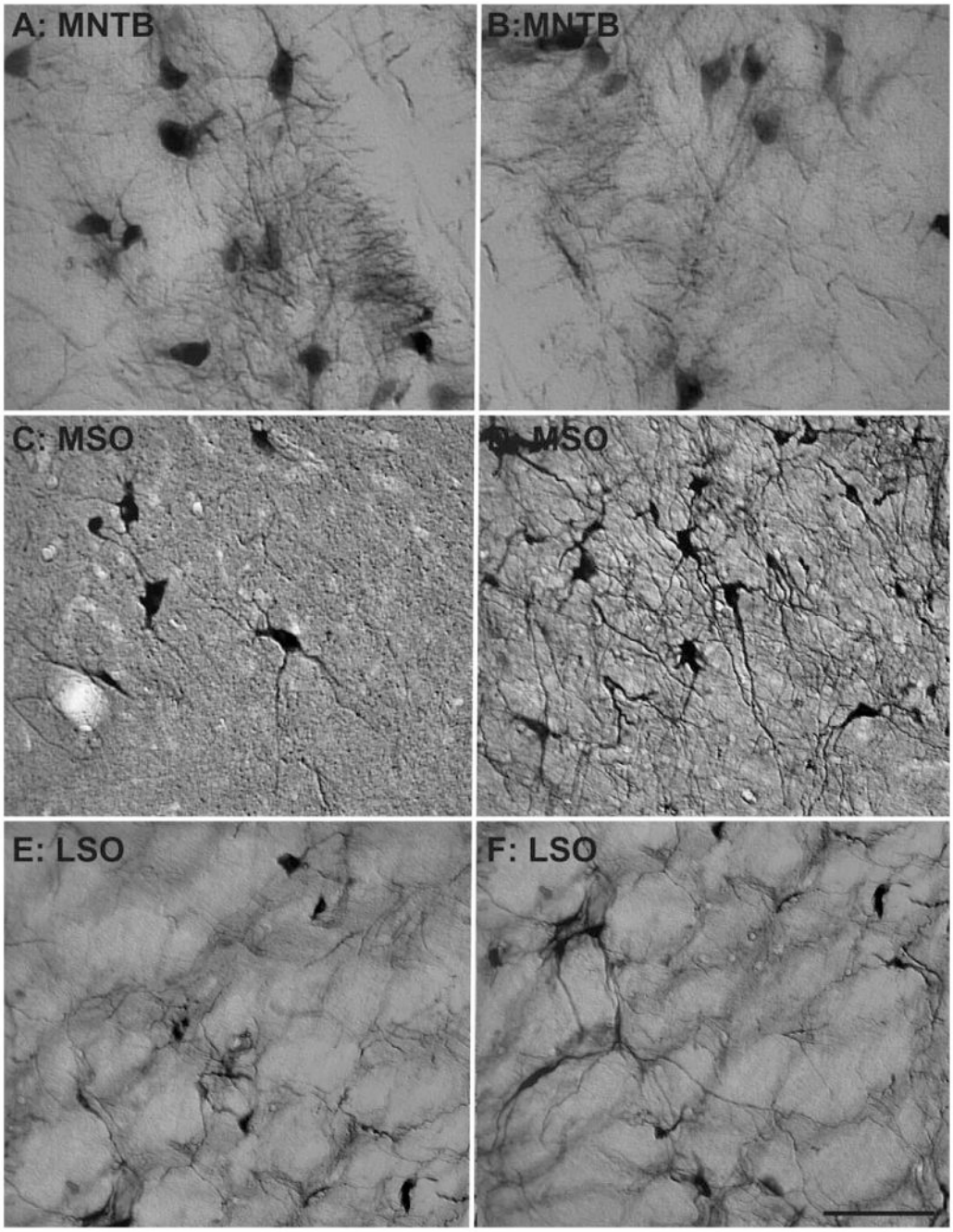

Figure 2.

Comparison of NADPHd cell density of the superior olivary complex between a 15- and a 35-year-old animal. Comparison of micrographs from a 15-year-old medial nucleus of the trapezoid body (MNTB; **A**) and a 35-year-old MNTB (**B**) reveals no apparent age-related changes in density. However, when comparing a 15-year-old medial superior olive (MSO; **C**) with a 35-year-old MSO (**D**), age-related density changes become apparent. Similar to the MNTB, the lateral superior olive (LSO) showed no clear age-related changes between

the 15-year-old (**E**) and the 35-year-old (**F**) animal. Dorsal is upward and medial toward the left. Scale bar = 100 μm.

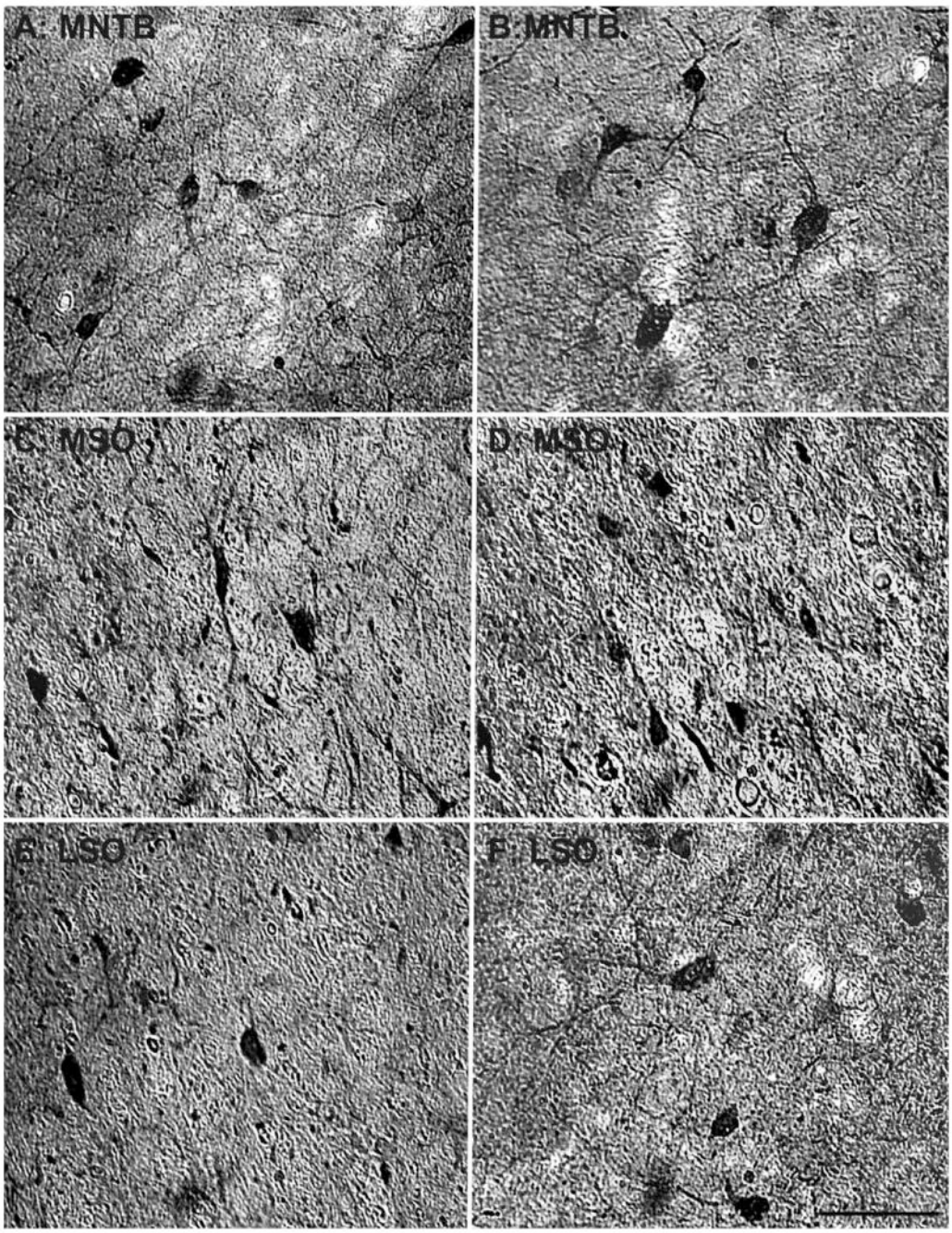

Figure 3.

Comparison of parvalbumin-positive cell density of the SOC between a 15- and a 35-year-old animal. Comparison of micrographs from a 15-year-old MNTB (**A**) and a 35-year-old MNTB (**B**) reveals no apparent age-related changes in density. However, when comparing a 15-year-old MSO (**C**) with a 35-year-old MSO (**D**), age-related density changes become apparent. Similar to the MNTB, the LSO showed no clear age-related changes between the 15-year-old (**E**) and the 35-year-old (**F**) animals. Conventions as in Figure 2. Scale bar = 100 μm.

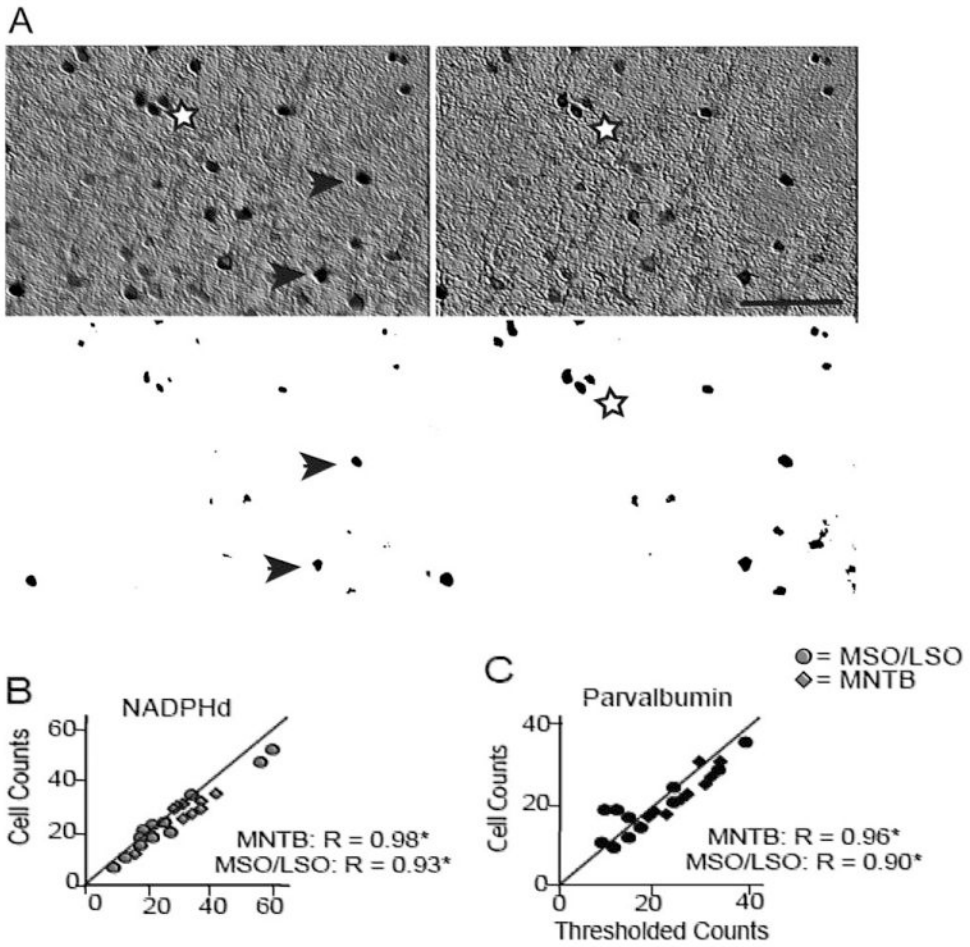

Figure 4.

Examples of the threshold analysis on histological sections to assess the observer's ability to differentiate positively labeled cells from background staining. **A:** Example of an analyzed section and its corresponding thresholded and binarized image at two different planes of the optical disector. In the left panel, arrows mark positively stained neurons counted at that plane, and the stars demarcate neurons that were counted when the optical plane moved (right panel). This sample is from the LSO, which along with the MSO showed strong background staining compared with the MNTB. Comparing NADPHd (**B**)- and parvalbumin (**C**)-positive cell counts and the counts from their thresholded pictures in the MNTB (lozenges) and the MSO/LSO (circles) revealed strong correlations, suggesting that the observers reliably differentiated labeled cells from the background. The MNTB served as a control in these comparisons because of its noticeably reduced background staining. Scale bar = 250 μm.

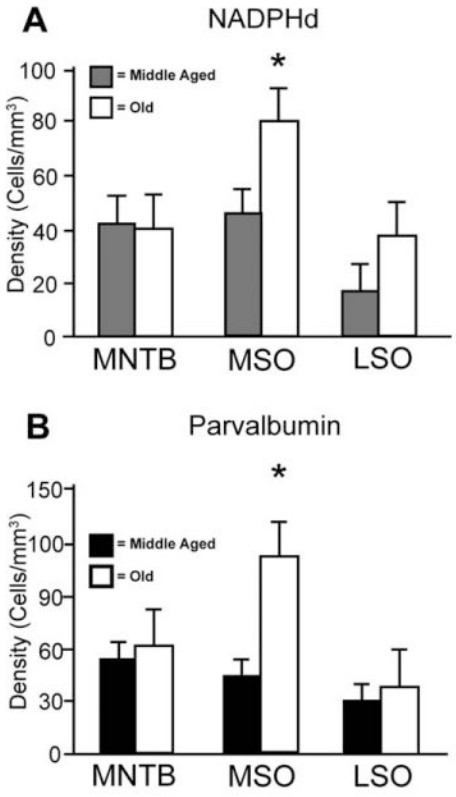

Figure 5.

Estimated cell densities from the three subdivisions of the SOC. Age-related comparisons of NADPHd (**A**)-positive and parvalbumin (PV; **A**)-positive cell densities in the medial nucleus of the trapezoid body (MNTB), medial superior olive (MSO), and lateral superior olive (LSO). Solid bars represent middle-aged density averages, and open bars represent density averages from aged animals. Significant increases of both NADPHd and PV were noted only within the MSO nucleus. *$P < 0.01$.

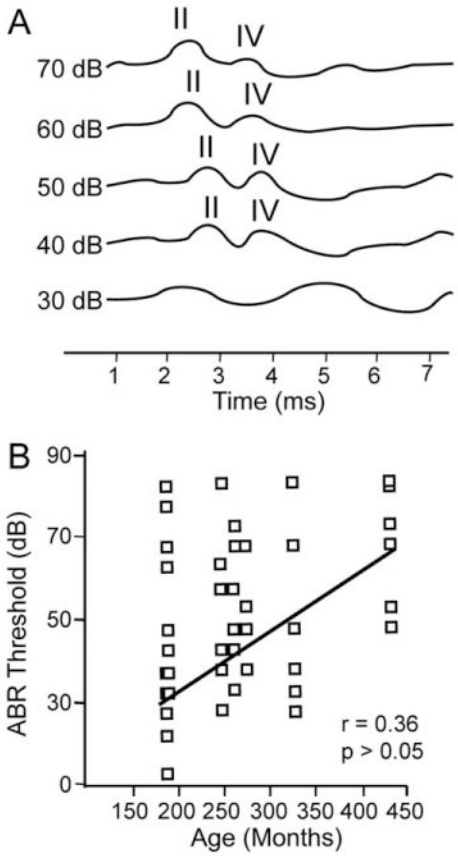

Figure 6.

Schematic auditory brainstem responses (ABRs). **A:** Reconstructed ABR from the left ear of a 15-year-old macaque with peaks II and IV labeled when present. **B:** ABR thresholds from the seven monkeys in which ABRs were collected for all stimuli (clicks and low-, middle-, and high-frequency tones). Threshold was defined as the last stimulus intensity in which wave II and wave IV were observable.

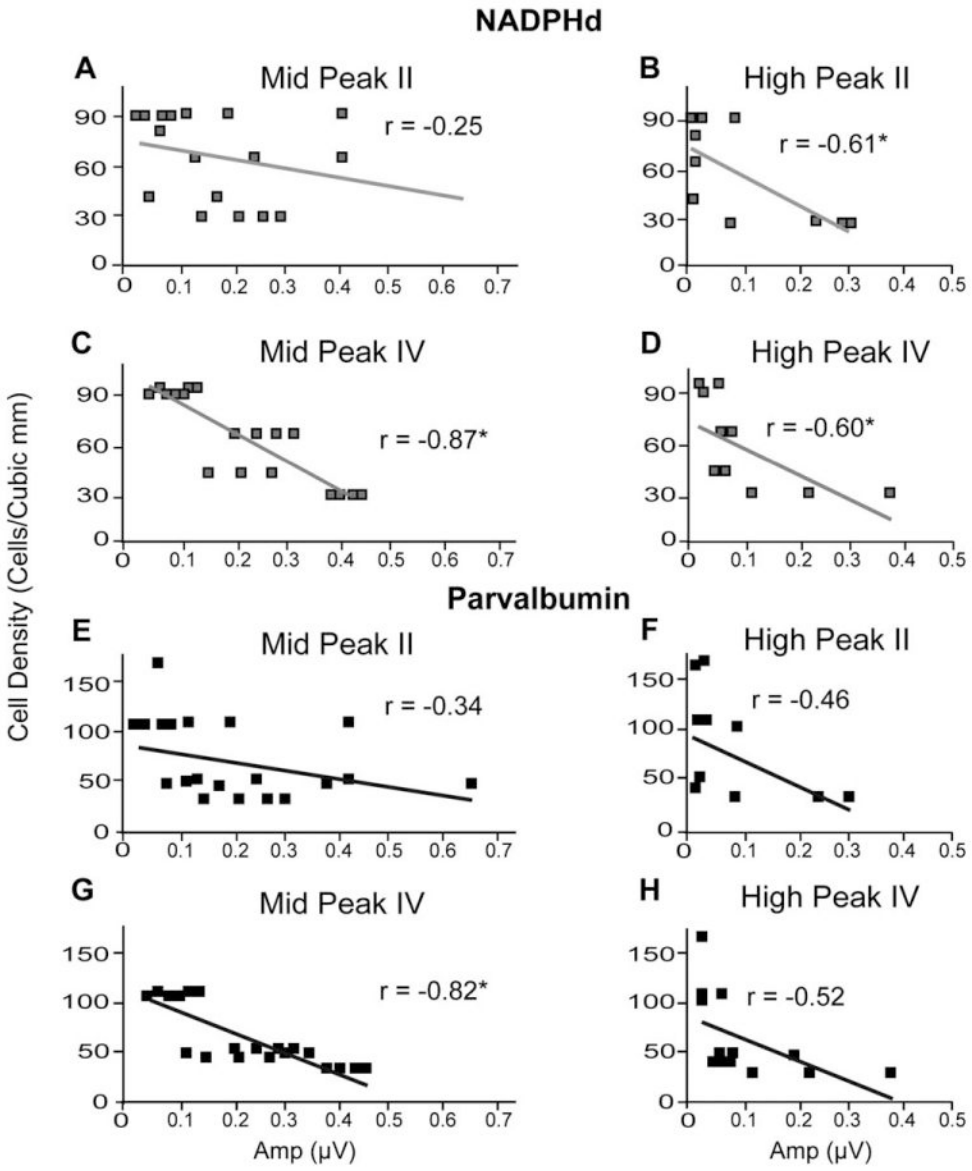

Figure 7.

Relationship between suprathreshold stimulus auditory brainstem response (ABR) amplitudes and cell density in the medial superior olive (MSO) at 70 dB SPL. Cell density of NADPHd (**A–D**)-positive cells and parvalbumin (**E–H**)-positive cells in the MSO as a function of peak II or IV ABR amplitudes using middle- and high-frequency tone stimuli (labeled accordingly) at 70 dB SPL. Few significant correlations were noted (B,D,H), suggesting that ABR responses to suprathreshold stimuli remain fairly constant regardless of the underlying chemical changes.

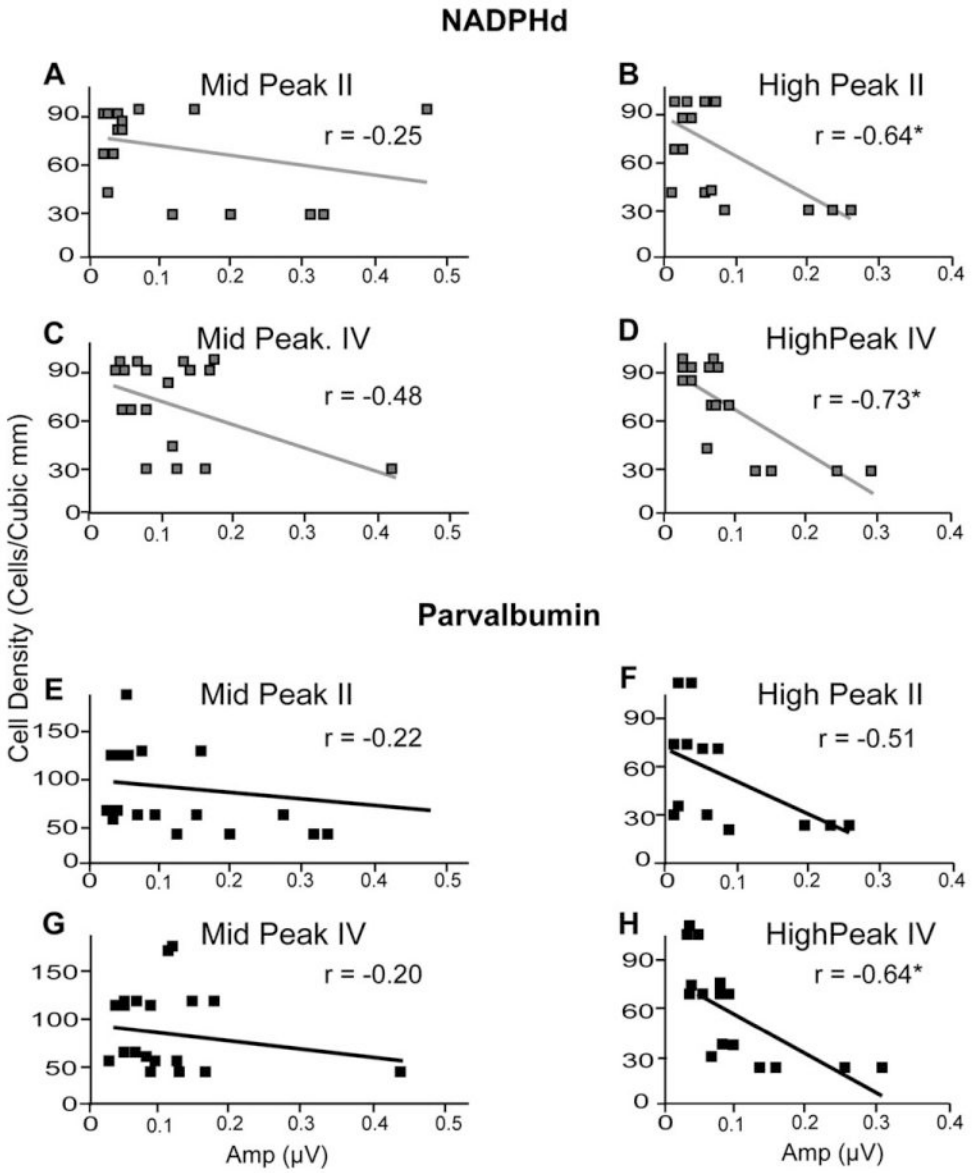

Figure 8.

Relationship between threshold stimulus auditory brainstem response (ABR) amplitudes and cell density in the medial superior olive (MSO) at the ABR threshold. Cell density of NADPHd (**A–D**)-positive cells and parvalbumin (**E–H**)-positive cells in the MSO following the conventions of Figure 7. Significant correlations were seen for some comparisons at this intensity (B–D,G). These correlations suggest that the ABR response to threshold tones differs as a function of cell density.

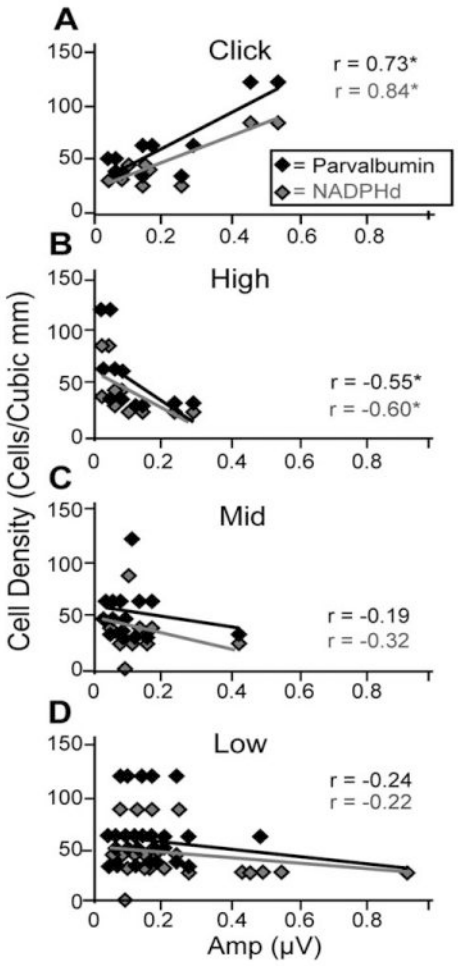

Figure 9.

Correlations between cell densities and threshold ABR amplitudes differ by stimulus type. The cell density of NADPHd-positive (gray) and parvalbumin (PV)-positive (black) cells combined from the principle nuclei of the superior olivary complex (SOC) as a function of peak IV amplitudes using click stimuli (**A**) or B) or high-frequency (**B**), middle-frequency (**C**), and low-frequency (**D**) tone stimuli. All stimuli were presented at threshold intensities. Note the inverse relationship between tones and cell density and the opposite trend with click stimuli. This observation suggests that tones and clicks are processed differently and that these differences correlate with chemical changes in the SOC.

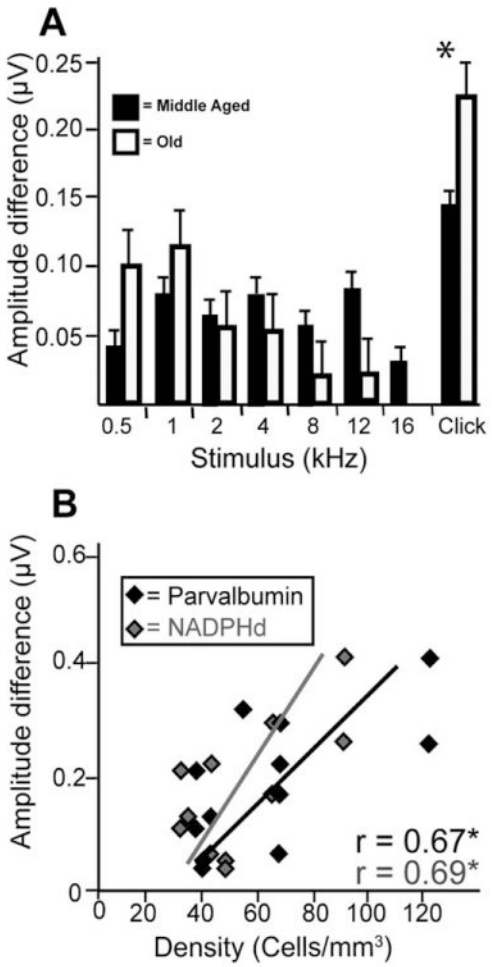

Figure 10.

ABR amplitude differences as a function of stimulus types and cell densities. **A:** The difference in auditory brainstem response amplitudes at 10 dB above threshold and at threshold using click and 0.5-, 1-, 2-, 4-, 8-, 12-, and 16-kHz tone stimuli in middle-aged (solid bars) and old (open bars) monkeys. The larger value observed with click stimuli suggests a steeper amplitude decrease for click stimuli leading down to threshold. This further suggests that clicks and tones are processed distinctly and can indirectly be noted through the ABR. **B:** Difference in auditory brainstem response amplitudes to clicks at 10 dB SPL above threshold and at threshold as a function of cell density. Correlations were significant for both stains. *$P < 0.05$.

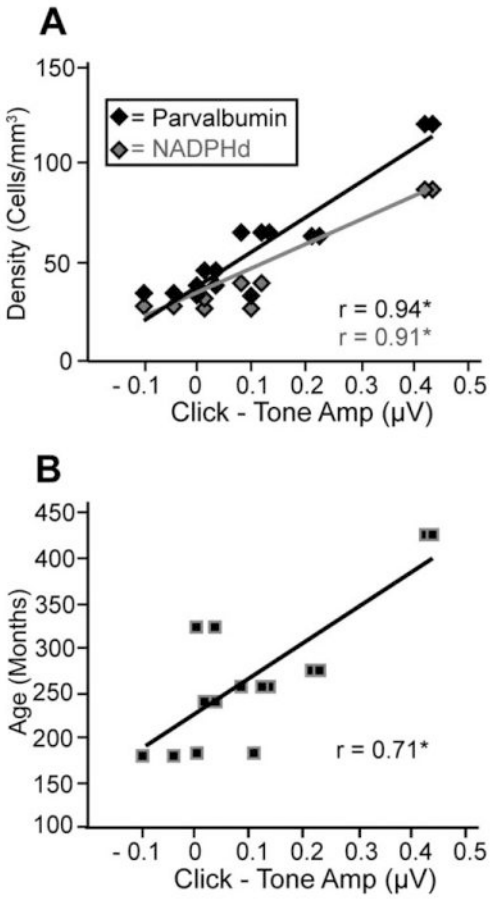

Figure 11.

Amplitude differences as a function of cell density and age. The difference between threshold amplitudes of clicks and high-frequency tone auditory brainstem responses as a function of cell density (**A**) and age (**B**). Higher values indicate greater prominence of click amplitudes over tones amplitudes at threshold. Again, this suggests that clicks and tones are processed differently and that the magnitude of this difference correlates with both cell density and age. Note that the x-axis is identical in both panels for direct comparison.

Table 1

Demographics, ABR, and Anatomical Methods Used in Monkeys

Age (months)	Human age (years)	Gender	ABR	Plane of section	Thickness (μm)	Auditory training
147	37	Male	No	Oblique	25	No
184	46	Male	Yes	Sagittal	40	No
185	46	Male	Yes	Oblique	30	No
243	61	Female	Yes	Oblique	50	Yes
267	67	Female	Yes	Oblique	50	No
276	69	Female	Yes	Oblique	50	No
324	81	Male	Yes	Oblique	40	Yes
427	107	Female	Yes	Oblique	25	No

Table 2

Information on the Antibodies and Chemicals Used for Immunohistochemical and Histochemical Reactions

	Antigen/chemical	Immunogen	Manufacturer/log No./other information
Parvalbumin immunohistochemistry	Mouse monoclonal antiparvalbuminclone PARV-19	Frog muscle parvalbumin	Sigma-Aldrich, P-3088
Parvalbumin immunohistochemistry	Biotinylated anti-mouse IgG	Mouse IgG	Vector, BA-2000; made in horse
Parvalbumin immunohistochemistry	Normal horse serum	N/A	Vector, S-2000
Parvalbumin immunohistochemistry	SG substrate Kit	N/A	Vector, SK-4700
NADPH-diaphorase histochemistry	Nitroblue tetrazolium	N/A	Sigma-Aldrich, N-6876
NADPH-diaphorase histochemistry	NADPH	N/A	Sigma-Aldrich, N-1630